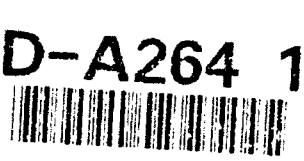

(2)

ARMY RESEARCH LABORATORY

A Thermoelastic Model for Thick Composite Rings

Jerome T. Tzeng

ARL-TR-105 May 1993

NOTICES

Destroy this report when it is no longer needed. DO NOT return it to the originator.

Additional copies of this report may be obtained from the National Technical Information Service, U.S. Department of Commerce, 5285 Port Royal Road, Springfield, VA 22161.

The findings of this report are not to be construed as an official Department of the Army position, unless so designated by other authorized documents.

The use of trade names or manufacturers' names in this report does not constitute indorsement of any commercial product.

REPORT DOCUMENTATION PAGE

Form Approved
OMB No 0704-0188

1. AGENCY USE ONLY (Leave blank)	2. REPORT DATE	3. REPORT TYPE AND DATES COVERED
	May 1993	Final, January 1991–March 1992

4. TITLE AND SUBTITLE

A Thermoelastic Model for Thick Composite Rings

5. FUNDING NUMBERS

C: DAALD3-86-D-0001

6. AUTHOR(S)

Jerome T. Tzeng

7. PERFORMING ORGANIZATION NAME(S) AND ADDRESS(ES)

U.S. Army Research Laboratory
ATTN: AMSRL-WT-PD
Aberdeen Proving Ground, MD 21005-5066

8. PERFORMING ORGANIZATION REPORT NUMBER

9. SPONSORING / MONITORING AGENCY NAME(S) AND ADDRESS(ES)

U.S. Army Research Laboratory
ATTN: AMSRL-OP-CI-B (Tech Lib)
Aberdeen Proving Ground, MD 21005-5066

10. SPONSORING / MONITORING AGENCY REPORT NUMBER

ARL-TR-105

11. SUPPLEMENTARY NOTES

12a. DISTRIBUTION / AVAILABILITY STATEMENT

Approved for public release; distribution is unlimited.

12b. DISTRIBUTION CODE

13. ABSTRACT *(Maximum 200 words)*

The thermoelastic response of a thick multilayered composite ring subjected to the sequential addition of layers which undergo instantaneous temperature change and corresponding thermal deformation is modeled. The analysis considers ply-by-ply variations of material properties and fiber orientations. The resulting residual stress field is examined as a function of important physical parameters such as ring geometry, layer material properties, fiber orientation, and layer sequence.

14. SUBJECT TERMS

composite structures; thermal stresses; filament winding

15. NUMBER OF PAGES

32

16. PRICE CODE

17. SECURITY CLASSIFICATION OF REPORT	18. SECURITY CLASSIFICATION OF THIS PAGE	19. SECURITY CLASSIFICATION OF ABSTRACT	20. LIMITATION OF ABSTRACT
UNCLASSIFIED	UNCLASSIFIED	UNCLASSIFIED	UL

INTENTIONALLY LEFT BLANK.

TABLE OF CONTENTS

		Page
	LIST OF FIGURES	v
	PREFACE	vii
1.	INTRODUCTION	1
2.	MODEL DEVELOPMENT	2
3.	RESULTS AND DISCUSSION	6
3.1	Results for Post-Consolidated (Hoop-Wound) Case	7
3.2	Results for In-Situ Consolidated (Hoop-Wound) Case	8
3.3	Results for Post-Consolidated (Bidirectional-Wound) Case	9
3.4	Results for In-Situ Consolidated (Bidirectional-Wound) Case	9
4.	CONCLUSIONS	10
5.	REFERENCES	23
	DISTRIBUTION LIST	25

INTENTIONALLY LEFT BLANK.

LIST OF FIGURES

Figure		Page
1.	Schematic of the in-situ consolidation winding process. For the post-consolidation process, components are consolidated by using an autoclave	12
2a.	Self-equilibrating condition of circumferential stress	13
2b.	Free-body diagrams for layer-by-layer force balance of radial and circumferential stresses in a two-layered ring	13
3.	Normalized stresses as layer number for post-consolidated hoop-wound graphite/TP ring	14
4.	Normalized stresses as layer number for post-consolidated hoop-wound glass/TP ring	15
5.	Normalized stresses as layer number for in-situ consolidated hoop-wound graphite/TP ring	16
6.	Normalized stresses as layer number for in-situ consolidated hoop-wound glass/TP ring	17
7.	Normalized stresses as layer number for post-consolidated bidirectional-wound graphite/TP ring	18
8.	Normalized stresses as layer number for post-consolidated bidirectional-wound glass/TP ring	19
9.	Normalized stresses as layer number for in-situ consolidated bidirectional-wound graphite/TP ring	20
10.	Normalized stresses as layer number for in-situ consolidated bidirectional-wound glass/TP ring	21

INTENTIONALLY LEFT BLANK.

PREFACE

The U.S. Army Ballistic Research Laboratory was deactivated on 30 September 1992 and subsequently became a part of the U.S. Army Research Laboratory (ARL) on 1 October 1992.

INTENTIONALLY LEFT BLANK.

1. INTRODUCTION

Thermoplastic filament winding can utilize in-situ consolidation as well as post-consolidation processes. Recently, thermoset composite can also be cured during winding and tape laying. A schematic of the winding process is given in Figure 1. In the process of in-situ consolidation, prepreg tow is simultaneously heated, cured, and consolidated onto a substrate or mandrel at the processing temperature. The temperature of each layer drops rapidly due to heat transfer into the mandrel or substrate and to the atmosphere. In the traditional post-consolidation process, composite components are first wound and then consolidated in an autoclave. Accordingly, the entire composite part is heated to the cure temperature, held there for the appropriate length of time, and then uniformly cooled to ambient temperature.

Of critical concern for creating thick-section composite components are the residual stress states resulting from fabrication and their influence on the mechanical performance of the components. It is important to understand the magnitude and distribution of these residual stresses since the stresses could be large enough to cause initial failure and may significantly reduce structural performance.

During processing, thermal stresses in composite rings are developed due to anisotropic thermal deformation and the so-called geometric effect arising from cylindrical geometry. The thermal residual stress state in an in-situ consolidated ring can be modeled by sequential addition of layers at a specified processing temperature with corresponding instantaneous thermal shrinkage or expansion of each layer.

Residual stress analysis usually assumes the entire structure to be subjected to a uniform temperature change (Reuter 1973; Tarnopol'skii and Bell 1983; Calius and Springer 1985; Hyer et al. 1986; Nguyen and Knight 1988; Luo and Sun 1989). Such an analysis is appropriate only for prediction of residual stresses in a post-consolidated ring and not for an in-situ consolidated ring. Cirino (1989) has proposed an in-situ consolidation model for thermoplastic winding. The analysis simulates the winding process as a sequential addition of concentric rings to the mandrel. Although Cirino's model can predict the state of stress in an orthotropic ring due to the effects of winding tension and consolidation, only hoop-wound composite rings were considered.

We therefore first seek to develop a model which will predict the residual stresses in rings resulting from the in-situ consolidation process for rings with variation of layer-to-layer material properties and fiber orientation. Secondly, we investigate the effects of variation in processing approach, (i.e., post and in-situ

consolidation), material properties, and stacking sequence on the residual stress state in bidirectional (0°/90°) composite rings.

2. MODEL DEVELOPMENT

The model employs a multiple-layer analysis formulation. Each layer of the laminated ring is treated as an element with its own material properties. Both winding angle and material properties may vary layer to layer. In the formulation, thermal deformation is assumed to result from a uniform temperature change in each layer; however, ply-by-ply variations in temperature change are allowed. The model also includes the presence of the mandrel, which can greatly influence residual stresses in the ring.

In the post-consolidation model, it is assumed that all the layers undergo the same temperature change simultaneously. For in-situ consolidation, each layer is assumed to undergo the temperature change sequentially. Thus, for the in-situ case, the calculations are carried out N times (once for each of the N layers) and residual stresses are then accumulated as each layer is added.

Assuming axial symmetry, the strain-displacement relationships for any layer in the laminated composite ring can be expressed in cylindrical coordinates as follows (Nowinski, 1978):

$$\varepsilon_r = \frac{du}{dr}, \tag{1a}$$

and

$$\varepsilon_\theta = \frac{u}{r}, \tag{1b}$$

where ε_r is the radial strain component, ε_θ is the circumferential strain component, u is the radial displacement, and r is the radial coordinate (Figure 2a).

Assuming plane stress conditions, the constitutive equations for an orthotropic material with thermal anisotropy become (in the cylindrical coordinates):

$$\varepsilon_r = \frac{1}{E_r}\sigma_r - \frac{\nu_{\theta r}}{E_\theta}\sigma_\theta + \alpha_r \Delta T, \tag{2a}$$

and

$$\varepsilon_\theta = \frac{-\nu_{r\theta}}{E_r}\sigma_r + \frac{1}{E_\theta}\sigma_\theta + \alpha_\theta \Delta T, \tag{2b}$$

where E_i and ν_{ij} are the corresponding direction moduli and Poisson's ratios, α_i are the coefficients of thermal expansion, and ΔT is the temperature change. Both the mechanical and thermal properties may vary with fiber orientations from layer to layer.

The equilibrium equation is:

$$\frac{d\sigma_r}{dr} + \frac{\sigma_r - \sigma_\theta}{r} = 0, \tag{3}$$

where σ_r and σ_θ are the radial and the circumferential stress components, respectively.

Substitution of Equation 1 and Equation 2 into Equation 3 yields:

$$r^2\frac{d^2u}{dr^2} + r\frac{du}{dr} - k^2u = C_1 r \Delta T,$$

where

$$k^2 = \frac{E_\theta}{E_r}$$

and

$$C_1 = (1 - \nu_{\theta r})\alpha_r + (\nu_{\theta r} - k^2)\alpha_\theta. \tag{4}$$

The complete solution of Equation 4 consists of homogeneous and particular solutions as follows:

$$u(r) = Ar^{k} + Br^{-k} + \frac{C_1}{1 - k^2} r\Delta T, \tag{5}$$

where A and B are constants to be determined.

From Equation 1, Equation 2, and Equation 5, the circumferential and radial stress components can be derived and given by:

$$\sigma_r = AC_2 r^{k-1} + BC_3 r^{-k-1} + C_4 \Delta T, \tag{6a}$$

and

$$\sigma_\theta = AC_2 r^{k-1} - BC_3 r^{-k-1} + C_4 \Delta T, \tag{6b}$$

where

$$C_2 = \frac{E_r(\nu_{\theta r} + k)}{(1 - \nu_{\theta r}\nu_{r\theta})},$$

$$C_3 = \frac{E_r(\nu_{\theta r} - k)}{(1 - \nu_{\theta r}\nu_{r\theta})},$$

and

$$C_4 = \frac{E_\theta(\alpha_r - \alpha_\theta)}{(1 - k^2)}.$$

material properties and geometry. The total number of constants to be determined for a ring of N layers is therefore 2N.

Boundary conditions include continuity of radial displacements and radial stresses at all layer interfaces, resulting in 2(N – 1) boundary conditions. Furthermore, surface tractions at the inner and outer surfaces of the ring complete the set of 2N boundary conditions needed to determine all the constants A^k and B^k.

The direct procedure to solve these simultaneous equations can be very tedious and time consuming. A very effective method was developed to reduce the equations in half and also to solve the problem systematically by computer. Consider the k-th layer in a multiple-layer ring. The radial displacements at the inner and outer surfaces are by substituting the respective radii into Equation 5 as follows:

$$\begin{Bmatrix} u_i^k \\ u_o^k \end{Bmatrix} = \begin{bmatrix} f_{11}^k(r_i) & f_{12}^k(r_i) \\ f_{21}^k(r_o) & f_{22}^k(r_o) \end{bmatrix} \begin{Bmatrix} A^k \\ B^k \end{Bmatrix} + \begin{Bmatrix} F_i^k(\Delta T, r_i) \\ F_o^k(\Delta T, r_o) \end{Bmatrix}. \tag{7}$$

Where u_i^k and u_o^k are the radial displacements at the inner and outer surface of the k-th layer, f_{ij} are functions of radial position, A^k and B^k are undetermined constants, and $F_i^k(\Delta T, r_i)$ and $F_o^k(\Delta T, r_o)$ result from the layer particular solution.

Solving for constants A^k and B^k in terms of the radial displacements at the inner and the outer surfaces and substituting the constants A^k and B^k into the Equation 6a yield the radial stress component as follows:

$$\begin{Bmatrix} \sigma_i^k \\ \sigma_o^k \end{Bmatrix} = \begin{bmatrix} g_{11}^k(r,\Delta T) & g_{12}^k(r,\Delta T) \\ g_{21}^k(r,\Delta T) & g_{22}^k(r,\Delta T) \end{bmatrix} \begin{Bmatrix} u_i^k \\ u_o^k \end{Bmatrix} + \begin{Bmatrix} G_i^k(\Delta T, r) \\ G_o^k(\Delta T, r) \end{Bmatrix}, \tag{8}$$

where g_{ij} are functions of the inner and outer radial position and temperature, u_i^k and u_o^k are the radial displacements at the inner and outer surface of the k-th layer, and $G_i^k(\Delta T, r)$ and $G_o^k(\Delta T, r)$ (which can be viewed as components of force vector in the finite element method) result from the particular solution. The "r" in Equation 8 represents both the inner and outer radial positions.

Imposing the radial stress continuity boundary conditions results in a set of N + 1 simultaneous algebraic equations which can be expressed in matrix format as follows:

$$\begin{bmatrix} k_{11} & k_{12} & k_{13}\cdots \\ k_{21} & k_{22} & k_{23}\cdots \\ k_{31} & k_{32} & k_{33}\cdots \\ \vdots & \vdots & \vdots \ddots \end{bmatrix} \begin{Bmatrix} U_1 \\ U_2 \\ U_3 \\ \vdots \end{Bmatrix} = \begin{Bmatrix} \bar{k}_1 \\ \bar{k}_2 \\ \bar{k}_3 \\ \vdots \end{Bmatrix}, \tag{9}$$

where k_{ij} terms are functions of the radial positions and temperature differences for each layer, and U_i are the radial displacements at the layer interfaces and the surfaces of the ring. The $\bar{k}_i$ are obtained from the particular solution. Equation 9 can be readily solved for the larger displacements. Once these values are in hand, radial and circumferential stresses for each layer can be computed from Equation 8.

3. RESULTS AND DISCUSSIONS

Thermal residual stress predictions were developed for a 100-layer composite ring with an inner radius of 88.9 mm (3.5 in) and a outer radius of 101.6 mm (4.0 in) (i.e., r/t = 8.0). Two layups were considered: all hoop [(90)100] and [(90/0/90)33/90]. Two material systems, "Graphite/TP" and "Glass/TP" composites, were examined. Table 1 lists the relevant material properties for these two material systems. Predictions were made for two processing conditions: post- and in-situ consolidation. Therefore, a total of eight conditions were studied.

The processing temperature for thermoplastic composite (such as PEEK, PEKK) is approximately 350° C. Accordingly, residual stress was calculated by assuming the rings to be subjected to a temperature change of −320° C. For the post-consolidation simulation, a uniform temperature difference was applied. For the in-situ consolidation simulation, the temperature difference was applied to each layer as it was added, and the final residual stress state was obtained by accumulation of the stresses calculated. The stress results were normalized by $\alpha_1 E_1 \Delta T$ for the composite material used in the analysis. Predictions of the model were verified by checking overall requirements as follows:

1. The circumferential stresses were integrated through the thickness of the ring. The stress resultant thereby computed must vanish since the ring was not externally loaded (Figure 2a).

Table 1. Material Properties

Graphite/TP Composite :	
Longitudinal Elastic Modulus, E_1	135 GPa
Transverse Elastic Modulus, E_2, E_3	9 GPa
Poisson's Ratio, ν_{12}	0.30
Poisson's Ratio, ν_{23}	0.30
Poisson's Ratio, ν_{31}	0.02
Longitudinal Coefficient of Thermal Expansion, α_1	-0.5×10^{-6} /°C
Transverse Coefficient of Thermal Expansion, α_2, α_3	$30. \times 10^{-6}$ /°C
Ply Thickness	0.127 mm

Glass/TP Composite :	
Longitudinal Elastic Modulus, E_1	60 GPa
Transverse Elastic Modulus, E_2, E_3	10 GPa
Poisson's Ratio, ν_{12}	0.27
Poisson's Ratio, ν_{23}	0.30
Poisson's Ratio, ν_{31}	0.045
Longitudinal Coefficient of Thermal Expansion, α_1	3.5×10^{-6} /°C
Transverse Coefficient of Thermal Expansion, α_2, α_3	$30. \times 10^{-6}$ /°C
Ply Thickness	0.127 mm

2. A free-body diagram of one-half of the ring shows that the radial stress resultant at the interface of the inner and outer rings must balance the resultant of the circumferential stresses in the free-body diagram (Figure 2b).

3.1 Results for Post-Consolidated (Hoop-Wound) Case. Figures 3 and 4 show the normalized radial and circumferential stress distributions resulting from post-consolidation in the hoop-wound Graphite/TP and Glass/TP, respectively. The stress distributions are very similar for these two cases. For example, the circumferential stress is tensile at the inside radius and gradually changes to compression at the outer radius. The radial stress is tensile through the thickness for both material systems.

The coefficient of thermal expansion (CTE) of Graphite/TP is negative in the fiber direction (i.e., $\alpha_\theta < 0$). Accordingly, an all-hoop wound graphite ring expands in the circumferential direction (i.e., $\varepsilon_\theta > 0$) when it is cooled down from elevated temperature. The positive CTE in the radial direction results in shrinkage in thickness and causes a gradient of the hoop strain through the thickness. Thermal residual stresses result from the anisotropy in CTE and moduli in the radial and hoop directions. The hoop stress is tensile at the inner radius and compressive at the outer radius. In addition, the radial stress will be tensile throughout the thickness.

The residual stress in the Glass/TP ring is also due to anisotropic thermal shrinkage as well as moduli in the radial and circumferential directions. Although both the radial and circumferential CTE's of the Glass/TP are positive, the residual stress distribution is quite similar to the distribution of the Graphite/TP ring. However, the magnitudes of the residual stresses are smaller since the anisotropy of the glass material ring is small compared to the graphite material.

3.2 Results for In-Situ Consolidated (Hoop-Wound) Case. Figures 5 and 6 show the normalized radial and circumferential stress distributions in all-hoop wound rings subjected to in-situ consolidation for Graphite/TP and Glass/TP, respectively. Mandrel effects were not considered in the analysis.

The difference in residual stress states for the two materials is primarily due to the sign of the tangential CTE. The negative CTE of Graphite/TP causes circumferential expansion as the layer is cooled. Therefore, the circumferential stress is tensile at the inner radius and compressive at the outer radius of the ring. From the radial force equilibrium shown in the free-body diagram in Figure 2b, the radial stress is shown to be tensile through the thickness.

For the Glass/TP case, the layers shrink in both radial and circumferential directions as they are cooled on the substrate. The thermal shrinkage compresses the ring, resulting in compression in the circumferential direction. In addition, the radial stresses are compressive through the thickness. The circumferential stress in the outer radius is shown to be tensile to satisfy equilibrium (Figure 2a).

In-situ consolidation is shown to yield lower magnitude residual stresses in the outer region of the rings as compared to post-consolidation. The in-situ process is thus particularly suitable for materials with positive CTE's (such as Glass/TP) since the shrinkage will aid in consolidation. In contrast, the expansion

of graphite fibers in the circumferential direction (fiber direction) may result in tensile radial stresses causing poor bonding and low shear strength of the ring.

3.3 Results for Post-Consolidated (Bidirectional-Wound) Case. The normalized radial and hoop stress distributions for Graphite/TP and Glass/TP rings with [(90/0/90)33/90] layups resulting from post consolidation are shown in Figure 7 and Figure 8, respectively. Residual stress states for these two material systems are quite similar. For example, the circumferential stresses are discontinuous and vary with fiber orientation through the thickness. A dramatic variation of circumferential stresses exists at the interface between the 0° and 90° layers due to the anisotropy of the CTE's and moduli. The radial stresses are continuous through the thickness; however, substantial variation also exists through the thickness. The through thickness variation of the radial stresses results directly from the variation of the circumferential stress in the layer. The phenomena can be explained from the radial force equilibrium as shown in Figure 2.

For polymeric composite materials, the CTE is generally considerably greater in the direction transverse to the fibers than in the fiber direction ($\alpha 1 << \alpha 2$). Accordingly, tensile circumferential stresses must occur in the 0° plies for both Graphite/TP and Glass/TP. Due to the polar geometry and thermal shrinkage in the ring thickness direction, the circumferential stress shows a gradient through the thickness. The stress gradient yields tensile circumferential stress in the inner region and compressive circumferential stress in the outer region. Because the tangential modulus is higher than the transverse modulus, the circumferential stress gradient is larger in the 90° layers than in the 0° layers. The radial stress component shows a greater variation at the outside radius than at the inside radius since it depends directly on the circumferential stress.

It is concluded that the shrinkage of ring thickness due to the positive CTE will always result in circumferential stresses with tension at the inside radius and compression at the outside radius for a ring processed by post consolidation. The circumferential stress distribution generates a moment and causes the ring to close if it is cut. The radial stress is tensile to balance the circumferential stress resultant.

3.4 Results for In-Situ Consolidated (Bidirectional-Wound) Case. Figures 9 and 10 show the normalized radial and circumferential stresses in the Graphite/TP and Glass/TP rings with [(90/0/90)33/90] layups subjected to sequential addition of layers undergoing instantaneous temperature change. The resulting stress distributions for these two cases are very similar. The circumferential stresses are

compressive at the inside radius but gradually change to tension at the outside radius. The radial stresses are compressive throughout for both rings.

As discussed previously, the residual stress state due to the in-situ consolidation results directly from the difference in the tangential and radial CTE's. For the Graphite/TP ring, the 0° layers shrink while the 90° layers expand in the circumferential direction as the composite layers cool. For the Glass/TP ring, both the 0° and 90° layers shrink since the CTE's are positive in both directions. The Graphite/TP CTE's are more highly anisotropic; therefore, the residual stress state of Graphite/TP ring shows more perturbations.

The total residual stress state is a summation of the contributions from all layers and thus should correlate with results for average material properties of the rings. The averaged CTE's were found to be positive in both the circumferential and radial directions for these two rings by using laminate theory. Accordingly, the stress state variations are quite similar for these two material systems but different in magnitude.

4. CONCLUSIONS

A thermomechanical model has been developed to predict the residual stress state in laminated rings subjected to sequential addition of layers undergoing instantaneous temperature change and corresponding thermal deformation. The model accounts for the ply-by-ply variation of material properties and fiber orientations. A very efficient numerical technique has been developed and applied to solve the multilayered ring problems of hundreds of layers. This involves the solution of a system of algebraic equations equal to the number of layers plus one. The numerical method is particularly useful for simulation of in-situ consolidation processes for hundreds of layers.

Significant differences in the residual stress state were found between rings created using the post- and in-situ consolidation processes. The distribution of stress for post-consolidated rings (e.g., Graphite/TP or Glass/TP rings with all-hoop or bidirectional layups) will always be tensile circumferential stress at the inside radius and compressive stress at the outside radius. A net moment results from the circumferential stress distribution causing ring closure if the ring is cut. Radial stresses are tensile for post-consolidated rings regardless of material or layup. The tensile radial stress state may result in delaminations during manufacturing due to the relatively low transverse strength of the material.

The thermal residual stresses for the rings processed by in-situ consolidation are reduced compared to post consolidates since the composite is cooled layer by layer with minimum curvature effects. For the Glass/TP rings, the positive CTE's in both fiber and transverse directions cause compressive radial stress in both hoop- and bidirectional-wound rings. The circumferential stress is compressive at the inside radius and tensile at the outside radius. Accordingly, a net moment results such that the rings may open if they are cut.

For the hoop-wound graphite ring (which has negative CTE in the fiber direction), the hoop layers expand as they are cooled. The expansion in the circumferential direction results in tensile radial stresses. The tensile radial stress is critical since the strength of composite may be very low during consolidation. The circumferential stress is tensile at the inside radius and compressive at the outside radius due to force equilibrium. For the bidirectional-wound graphite rings, the residual stress state depends on average properties of the ring. The averaged CTE's are positive in both circumferential and radial directions; therefore, thermal stress distributions are similar to the bidirectional-wound glass ring.

A fundamental understanding of the thermal residual stress was obtained for post- and in-situ consolidation although the analyses do not include the effects from the winding tension and mandrel. Both the material properties (Table 1) and fabrication methods are shown to have great influence on the residual stress state. The developed model may be used for choosing layup construction, materials, and manufacturing process to achieve minimum residual stress state.

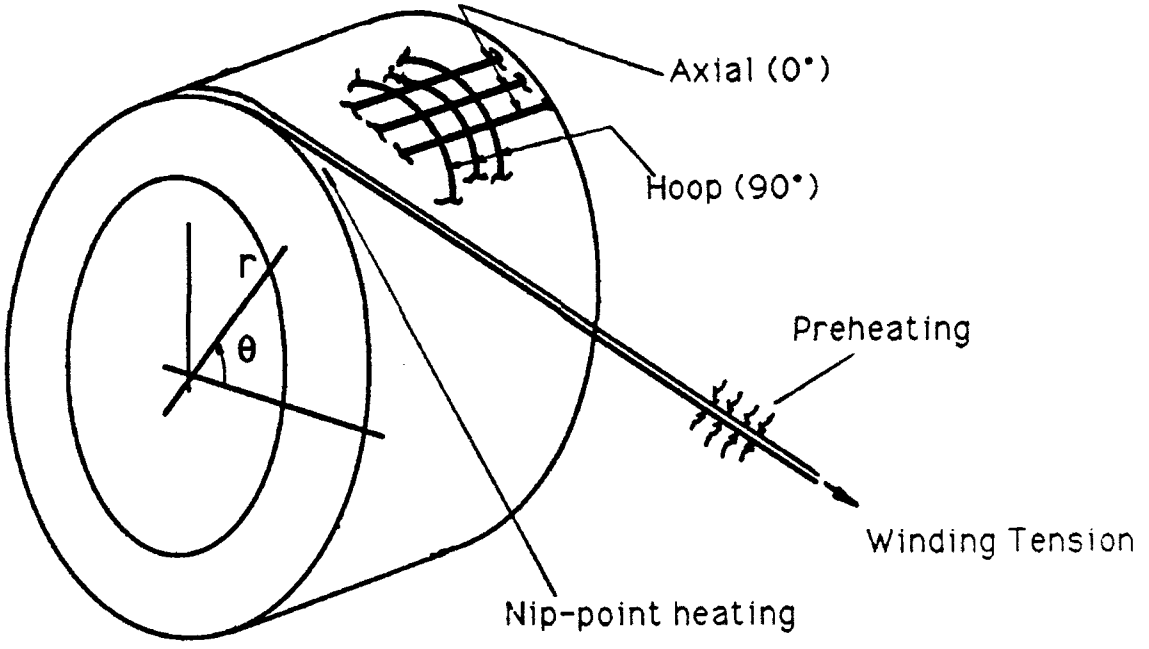

Figure 1. Schematic of the in-situ consolidation winding process. For the post-consolidation winding process, components are consolidated by using an autoclave.

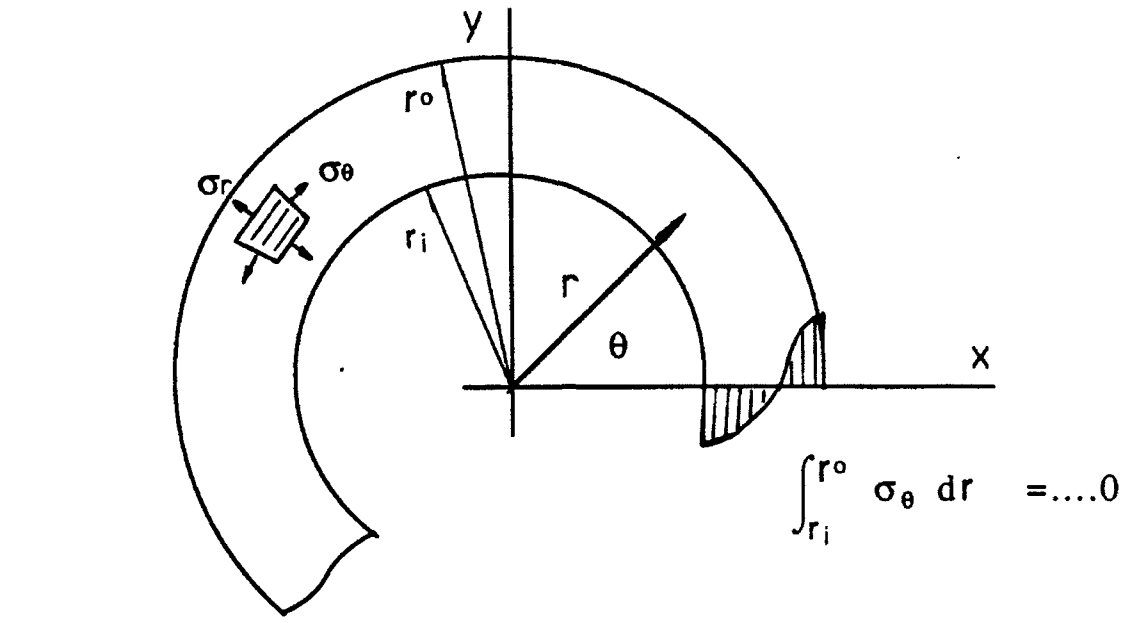

(a)

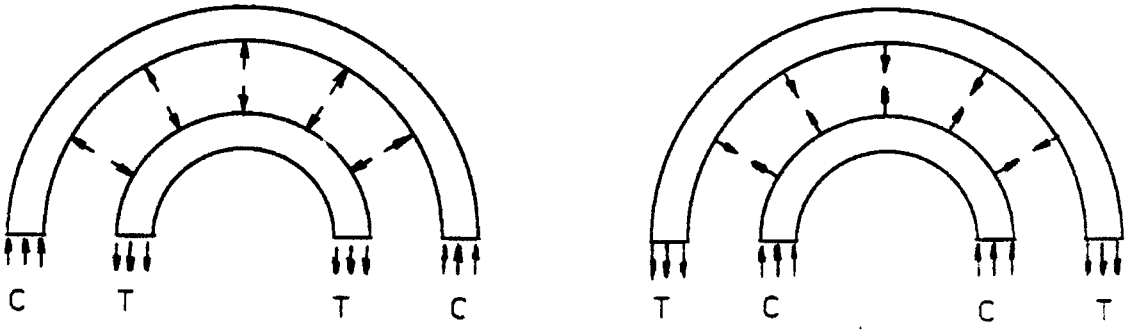

(b)

Figure 2. (a) Self-equilibrating condition of circumferential stress. (b) Free-body diagrams for layer-by-layer force balance of radial and circumferential stresses in a two-layered ring.

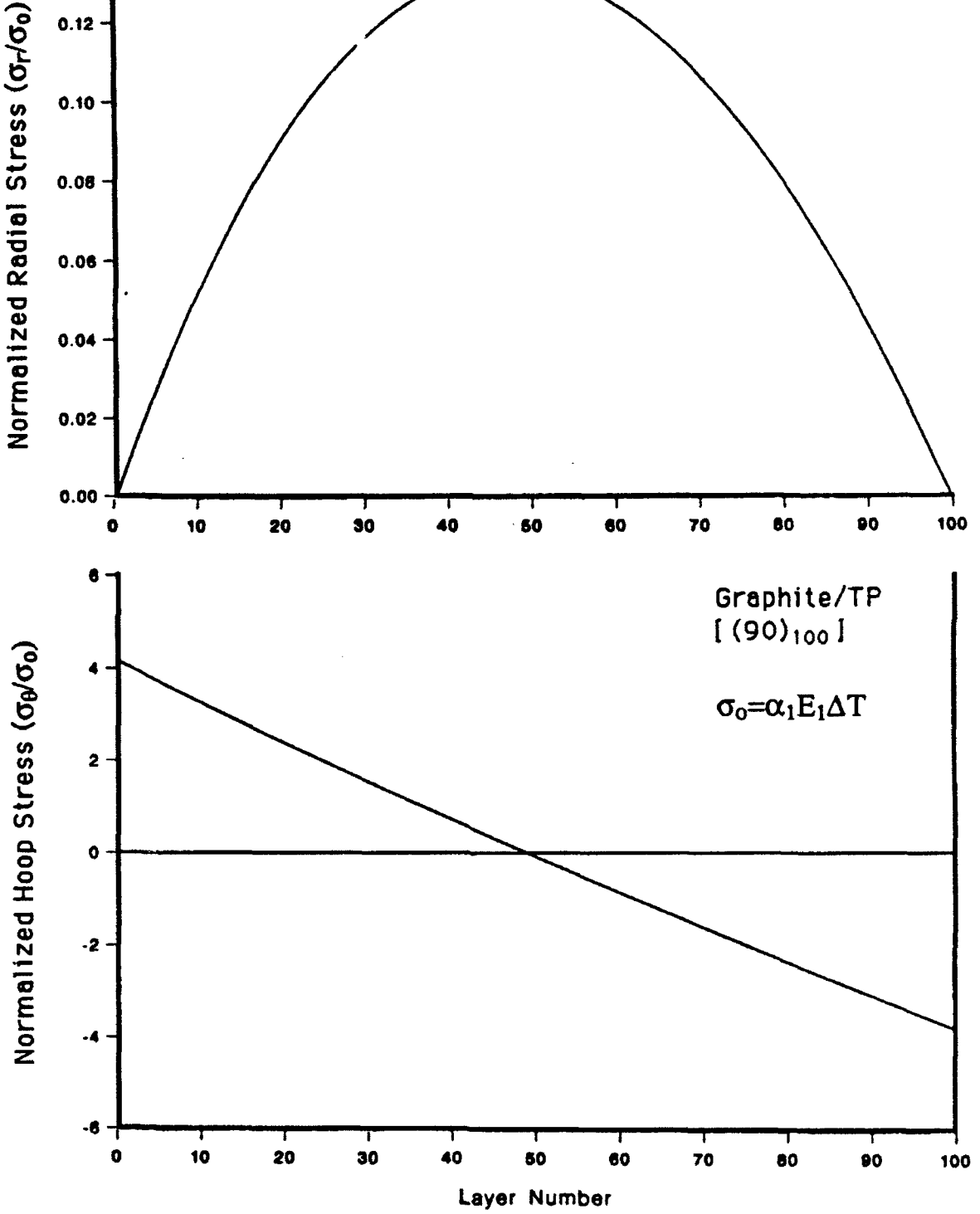

Figure 3. Normalized stresses as layer number for post-consolidated hoop-wound graphite/TP ring.

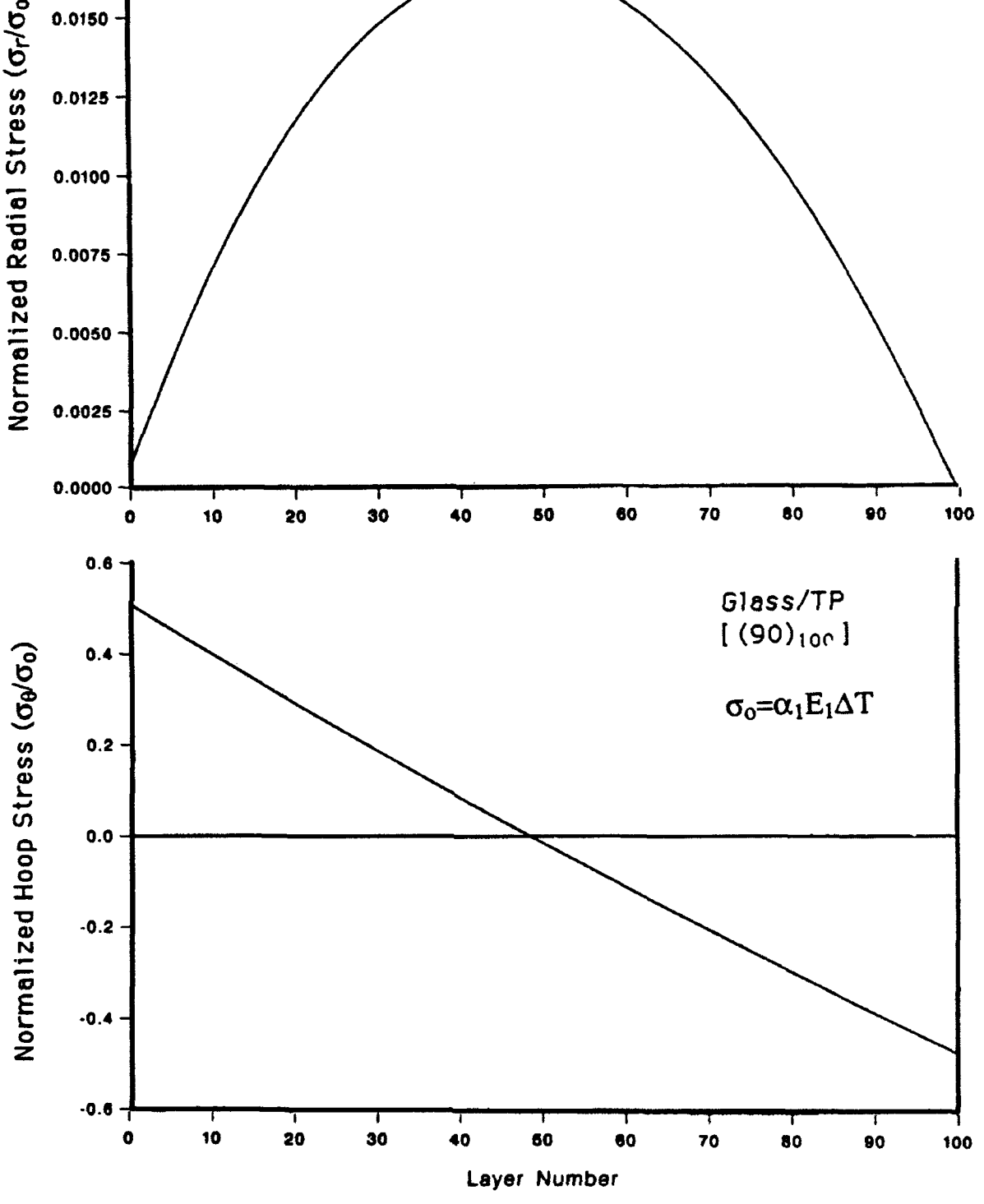

Figure 4. Normalized stresses as layer number for post-consolidated hoop-wound glass/TP ring.

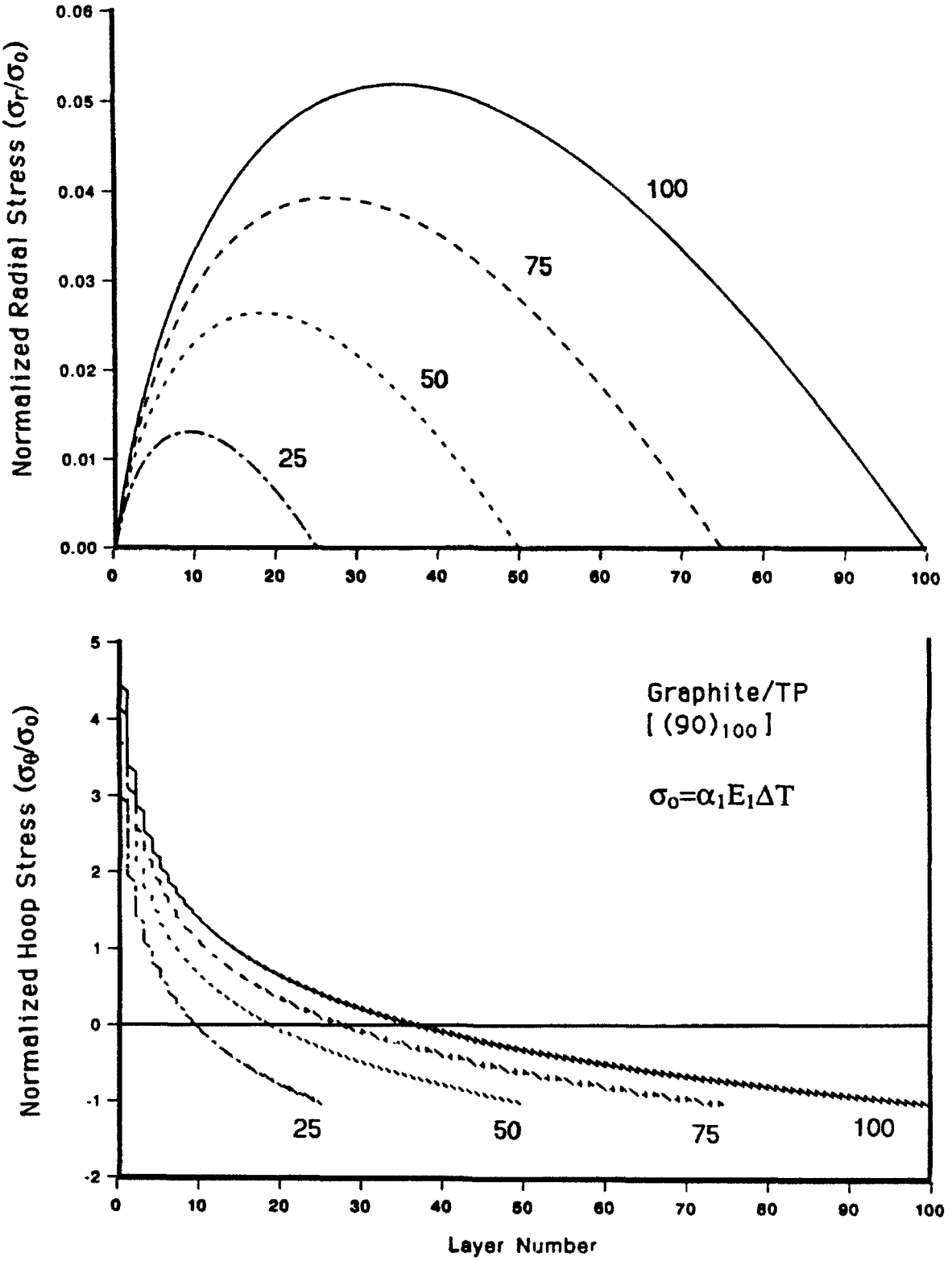

Figure 5. Normalized stresses as layer number for in-situ consolidated hoop-wound graphite/TP ring.

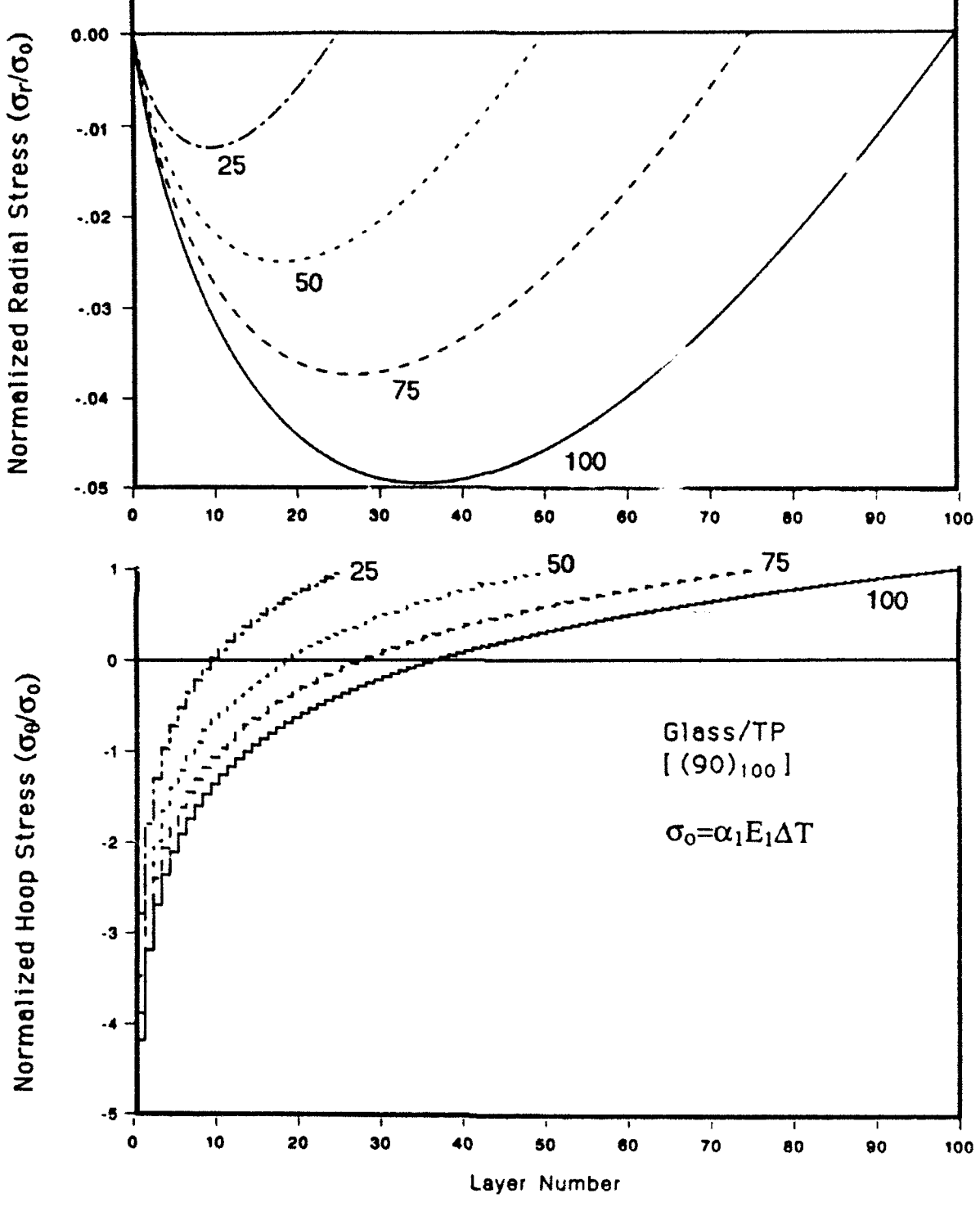

Figure 6. Normalized stresses as layer number for in-situ consolidated hoop-wound glass/TP ring.

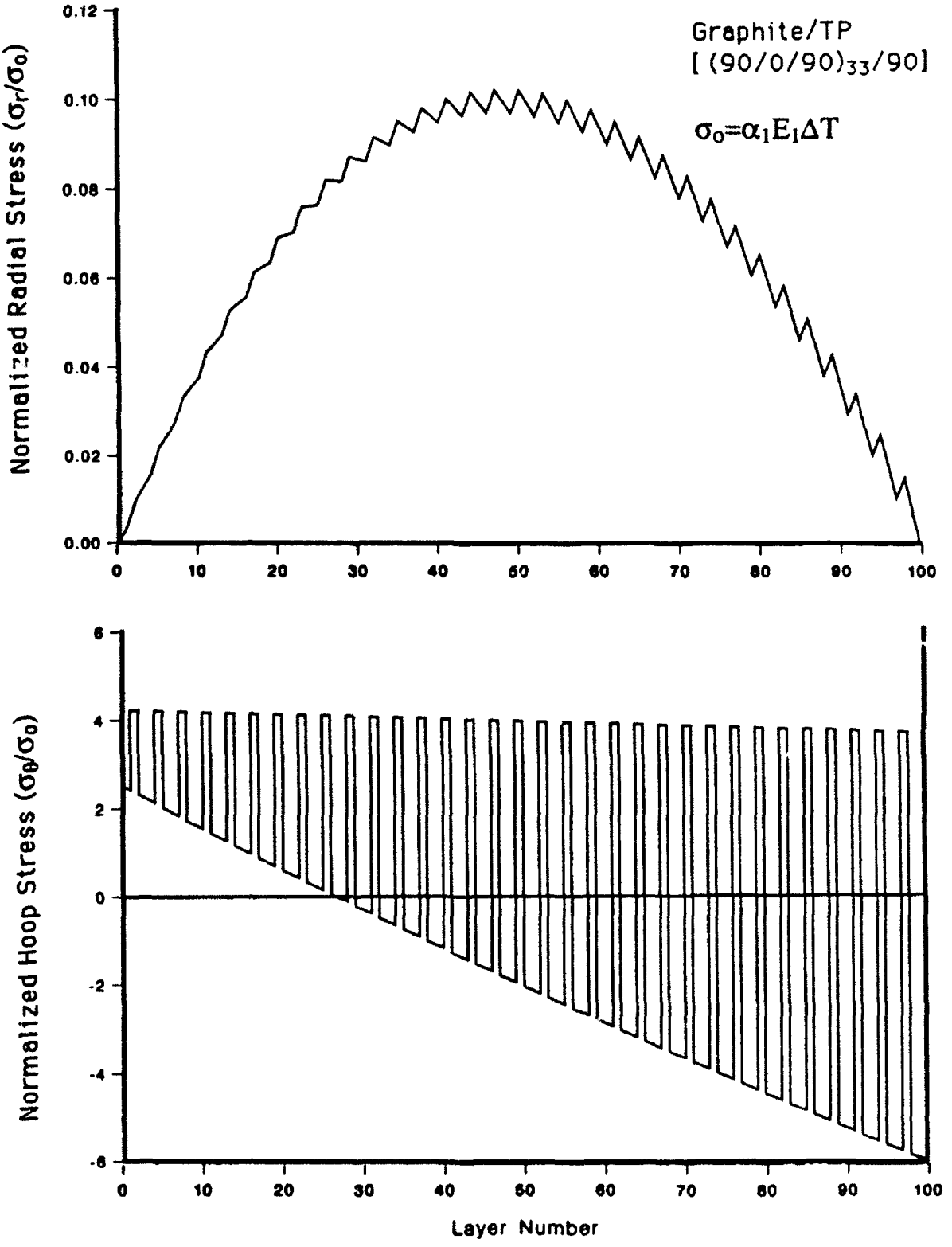

Figure 7. Normalized stresses as layer number for post-consolidated bidirectional-wound graphite/TP ring.

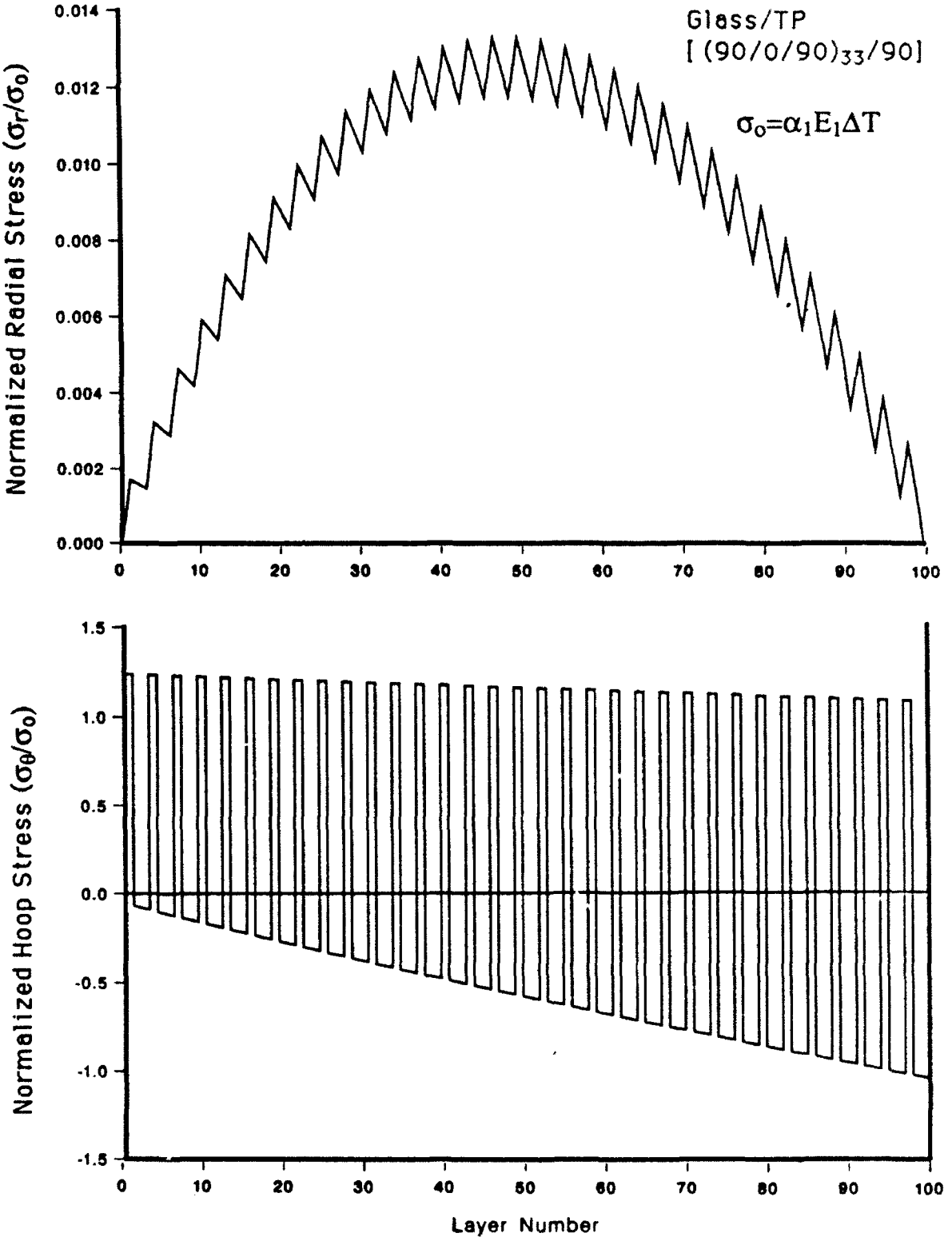

Figure 8. Normalized stresses as layer number for post-consolidated bidirectional-wound glass/TP ring.

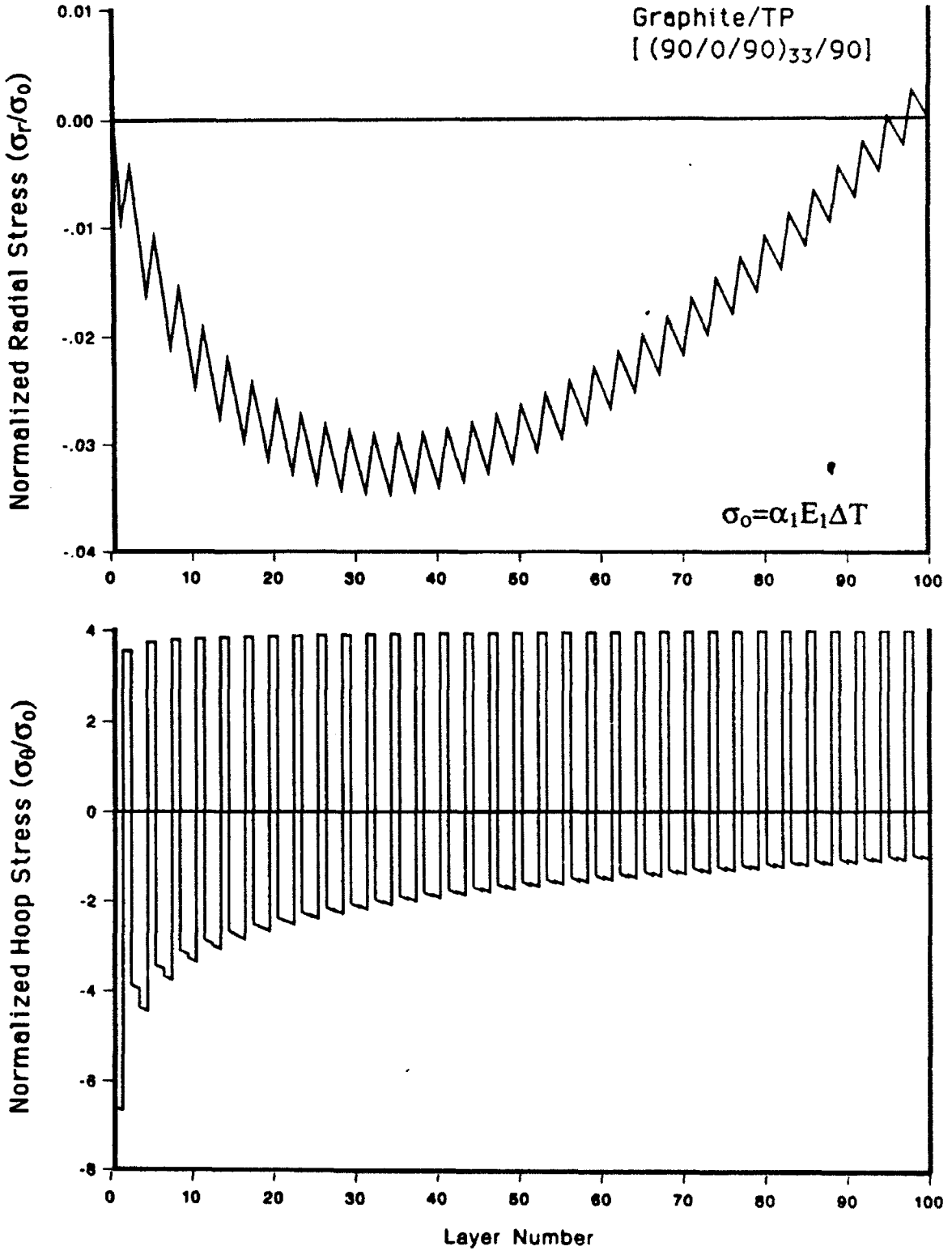

Figure 9. Normalized stresses as layer number for in-situ consolidated bidirectional-wound graphite/TP ring.

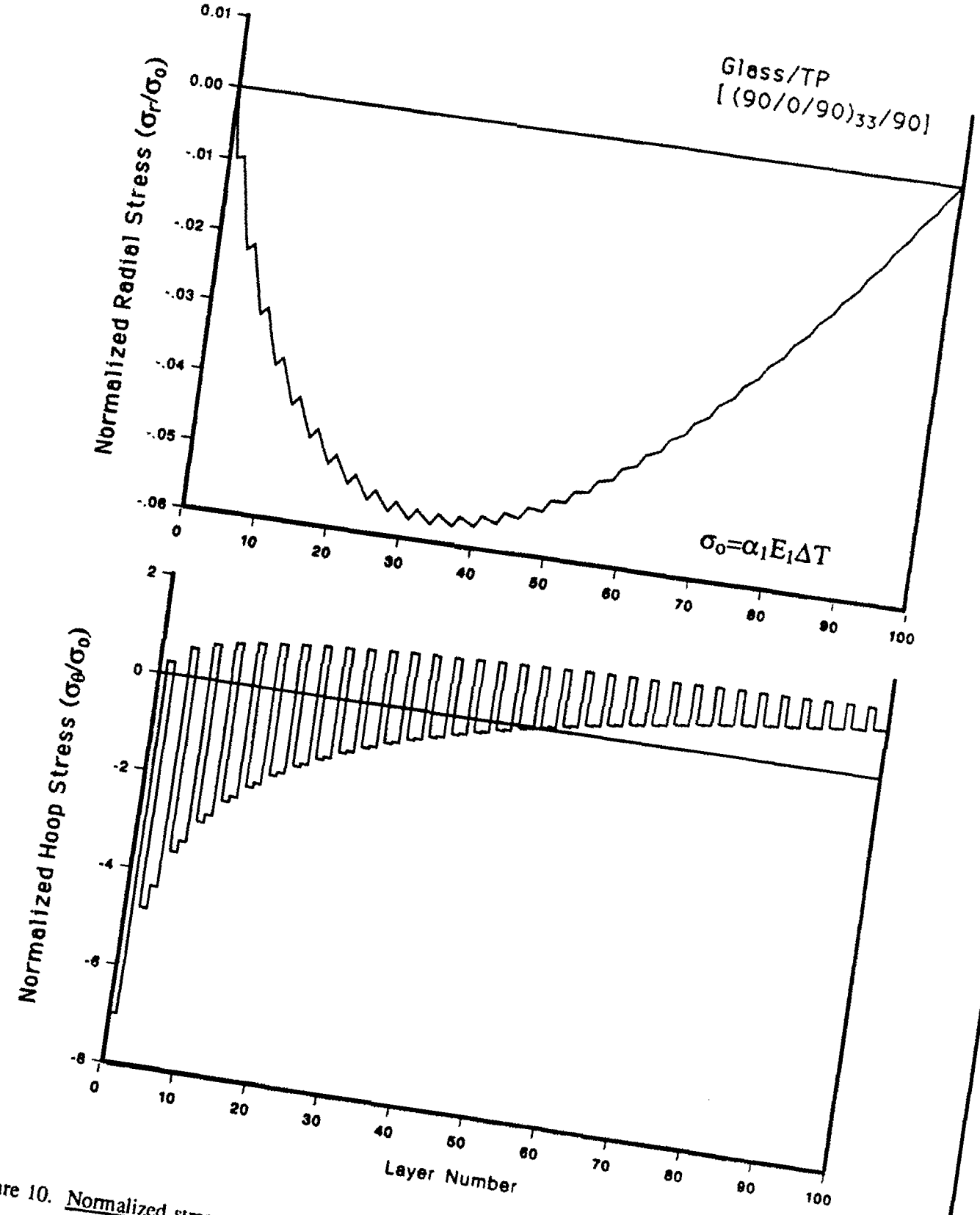

Figure 10. Normalized stresses as layer number for in-situ consolidated bidirectional-wound glass/TP ring.

INTENTIONALLY LEFT BLANK.

5. REFERENCES

Calius, E. P., and G. S. Springer. "Modeling the Filament Winding Process." Proceedings of the 15th International Conference on Composite Materials, W. C. Harrigan et al., ed., pp. 1071–1088, 1985.

Cirino, M. "Axisymmetric and Cylindrically Orthotropic Analysis of Filament Winding." Ph.D. Thesis, University of Delaware, Newark, DE, 1989.

Hyer, M. W., D. E. Cooper, and D. Cohen. "Stress and Deformation in Cross Ply Composite Tube Subjected to a uniform Temperature Change." Journal of Thermal Stresses, vol. 9, pp. 97–117, 1986.

Luo, J., and C. T. Sun. "Global-Local Methods for Thermoelastic Stress Analysis of Thick Fiber-Wound Cylinders." Proceedings of the 4th American Society for Composites, pp. 535–544, Blacksburg, VA, 1989.

Nguyen, V. D., and C. E. Knight. "A Fabrication Stress Model for Filament Wound Composites." Technical Report to Morton Thiokol, Inc., Aerospace Group, Brigham City, Utah, 1988.

Nowinski, J. L. Theory of Thermoelasticity With Applications. New York: Sijthoff & Noordhoff International Publishers, 1978.

Reuter, R. C., Jr. "Prediction and Control of Macroscopic Fabrication Stresses in Hoop Wound Fiberglass Rings." Analysis of the Test Method for High Modulus Fibers and Composites, ASTM STP 521, American Society for Testing and Materials, pp. 264–276, 1973.

Tarnopol'skii, Y. M., and A. I. Bell. "Problems of the Mechanics of Composite Winding." Handbook of Composites, vol. 4, pp. 45–108, 1983.

INTENTIONALLY LEFT BLANK.

No. of Copies	Organization
2	Administrator Defense Technical Info Center ATTN: DTIC-DDA Cameron Station Alexandria, VA 22304-6145
1	Commander U.S. Army Materiel Command ATTN: AMCAM 5001 Eisenhower Ave. Alexandria, VA 22333-0001
1	Director U.S. Army Research Laboratory ATTN: AMSRL-OP-CI-AD, Tech Publishing 2800 Powder Mill Rd. Adelphi, MD 20783-1145
1	Director U.S. Army Research Laboratory ATTN: AMSRL-OP-CI-AD, Records Management 2800 Powder Mill Rd. Adelphi, MD 20783-1145
2	Commander U.S. Army Armament Research, Development, and Engineering Center ATTN: SMCAR-IMI-I Picatinny Arsenal, NJ 07806-5000
2	Commander U.S. Army Armament Research, Development, and Engineering Center ATTN: SMCAR-TDC Picatinny Arsenal, NJ 07806-5000
1	Director Benet Weapons Laboratory U.S. Army Armament Research, Development, and Engineering Center ATTN: SMCAR-CCB-TL Watervliet, NY 12189-4050
(Unclass. only) 1	Commander U.S. Army Rock Island Arsenal ATTN: SMCRI-IMC-RT/Technical Library Rock Island, IL 61299-5000
1	Director U.S. Army Aviation Research and Technology Activity ATTN: SAVRT-R (Library) M/S 219-3 Ames Research Center Moffett Field, CA 94035-1000

No. of Copies	Organization
1	Commander U.S. Army Missile Command ATTN: AMSMI-RD-CS-R (DOC) Redstone Arsenal, AL 35898-5010
1	Commander U.S. Army Tank-Automotive Command ATTN: ASQNC-TAC-DIT (Technical Information Center) Warren, MI 48397-5000
1	Director U.S. Army TRADOC Analysis Command ATTN: ATRC-WSR White Sands Missile Range, NM 88002-5502
1	Commandant U.S. Army Field Artillery School ATTN: ATSF-CSI Ft. Sill, OK 73503-5000
(Class. only) 1	Commandant U.S. Army Infantry School ATTN: ATSH-CD (Security Mgr.) Fort Benning, GA 31905-5660
(Unclass. only) 1	Commandant U.S. Army Infantry School ATTN: ATSH-CD-CSO-OR Fort Benning, GA 31905-5660
1	WL/MNOI Eglin AFB, FL 32542-5000
	Aberdeen Proving Ground
2	Dir, USAMSAA ATTN: AMXSY-D AMXSY-MP, H. Cohen
1	Cdr, USATECOM ATTN: AMSTE-TC
1	Dir, ERDEC ATTN: SCBRD-RT
1	Cdr, CBDA ATTN: AMSCB-CI
1	Dir, USARL ATTN: AMSRL-SL-I
10	Dir, USARL ATTN: AMSRL-OP-CI-B (Tech Lib)

No. of Copies	Organization
11	Director Benet Laboratory U.S. Army Armament Research, Development, and Engineering Center ATTN: SMCAR-CCB, F. Heizer J. Keane T. Allen J. Vasilakis G. Friar J. Zweig T. Simkins V. Montvori J. Wrzochalski G. D'Andrea R. Hasenbein Watervliet, NY 12189-4050
1	Commander Watervliet Arsenal ATTN: SMCWV-QAE-Q, C. Howard Watervliet, NY 12189-4050
1	Commander Watervliet Arsenal ATTN: SMCWV-SPM, T. McCloskey Watervliet, NY 12189-4050
9	Commander U.S. Army Armament Research, Development, and Engineering Center ATTN: SMCAR-CCH-T, S. Musalli P. Christian K. Fehsal N. Krasnow R. Carr SMCAR-CCH-V, E. Fennell SMCAR-CCH-P, J. Lutz SMCAR-CCH, J. DeLorenzo SMCAR-CC, J. Hedderich Picatinny Arsenal, NJ 07806-5000

No. of Copies	Organization
3	Commander U.S. Army Armament Research, Development, and Engineering Center ATTN: SMCAR-TD, R. Price V. Linder T. Davidson Picatinny Arsenal, NJ 07806-5000
1	Commander Production Base Modernization Activity U.S. Army Armament Research, Development, and Engineering Center ATTN: AMSMC-PBM-K Picatinny Arsenal, NJ 07806-5000
1	Commander U.S. Army Belvoir RD&E Center ATTN: STRBE-JBC, C. Kominos Fort Belvoir, VA 22060-5606
2	Commander U.S. Army Missile Command ATTN: AMSMI-RD, W. McCorkle AMSMI-RD-ST, P. Doyle Redstone Arsenal, AL 35898
3	Commander U.S. Army Armament Research, Development, and Engineering Center ATTN: SMCAR-FSA-M, R. Botticelli F. Diorio SMCAR-FSA, C. Spinelli Picatinny Arsenal, NJ 07806-5000
3	Project Manager Advanced Field Artillery System ATTN: COL Napoliello LTC A. Ellis G. DelCoco Picatinny Arsenal, NJ 07806-5000
1	Commander Watervliet Arsenal ATTN: SMCWV-QA-QS, K. Insco Watervliet, NY 12189-4050

No. of Copies	Organization
2	Project Manager SADARM Picatinny Arsenal, NJ 07806-5000
7	Project Manager Tank Main Armament Systems ATTN: SFAE-AR-TMA, COL Hartline C. Kimker SFAE-AR-TMA-MD, H. Yuen J. McGreen SFAE-AR-TMA-ME, R. Joinson D. Guzowitz SFAE-AR-TMA-MP, W. Lang Picatinny Arsenal, NJ 07806-5000
1	U.S. Army Research Laboratory Advanced Concepts and Plans ATTN: AMSRL-CP-CA, D. Snider 2800 Powder Mill Road Adelphi, MD 20783
1	U.S. Army Materiel Command ATTN: AMCDCG-T, R. Chait 5001 Eisenhower Avenue Alexandria, VA 22333-0001
2	PEO-Armaments ATTN: SFAE-AR-PM, D. Adams T. McWilliams Picatinny Arsenal, NJ 07806-5000
2	U.S. Army Research Office Dir., Math & Computer Sciences Div. ATTN: Andrew Crowson AMXRO-MCS, J. Chandra P.O. Box 12211 Research Triangle Park, NC 27709-2211
2	NASA Langley Research Center Mail Stop 266 ATTN: F. Bartlett, Jr. AMSRL-VS, W. Elber Hampton, VA 23681-0001

No. of Copies	Organization
1	Commander Wright-Patterson Air Force Base ATTN: AFWAML, R. Kim Dayton, OH 45433
2	Commander DARPA ATTN: J. Kelly B. Wilcox 3701 North Fairfax Drive Arlington, VA 22203-1714
6	Director U.S. Army Research Laboratory Materials Technology Directorate ATTN: AMSRL-MA-P, L. Johnson B. Halpin T. Chou AMSRL-MA-PA, D. Granville W. Haskell AMSRL-MA-MA, G. Hagnauer Watertown, MA 02172-0001
9	Director U.S. Army Research Laboratory Weapons Technology Directorate ATTN: AMSRL-WT-PD (ALC), A. Abrahamian K. Barnes M. Berman H. Davison A. Frydman T. Li W. McIntosh E. Szymanski H. Watkins 2800 Powder Mill Road Adelphi, MD 20783-1145
1	Naval Research Laboratory Code 6383 ATTN: I. Wolock Washington, DC 20375-5000
1	Office of Naval Research Mech Div Code 1132SM ATTN: Yapa Rajapakse Arlington, VA 22217

No. of Copies	Organization
2	David Taylor Research Center ATTN: R. Rockwell W. Phyillaier Bethesda, MD 20054-5000
1	David Taylor Research Center Ship Structures and Protection Department ATTN: J. Corrado, Code 1702 Bethesda, MD 20084
4	Director Lawrence Livermore National Laboratory ATTN: R. Christensen S. de Teresa W. Feng F. Magness P.O. Box 808 Livermore, CA 94550
2	Pacific Northwest Laboratory A Div of Battelle Memorial Inst. Technical Information Section ATTN: M. Smith M. Garnich P.O. Box 999 Richland, WA 99352
6	Director Sandia National Laboratories Applied Mechanics Department, Division 8241 ATTN: C. Robinson G. Benedetti W. Kawahara K. Perano D. Dawson P. Nielan P.O. Box 969 Livermore, CA 94550-0096
1	Director Los Alamos National Laboratory ATTN: D. Rabern MEE-13, Mail Stop J-576 P.O. Box 1633 Los Alamos, NM 87545

No. of Copies	Organization
2	Virginia Polytechnical Institute and State University Dept of ESM ATTN: Michael W. Hyer Kenneth L. Reifsnider Blacksburg, VA 24061-0219
2	University of Dayton Research Institute ATTN: Ran Y. Kim Ajit K. Roy 300 College Park Avenue Dayton, OH 45469-0168
1	Drexel University ATTN: Albert S. D. Wang 32nd and Chestnut Streets Philadelphia, PA 19104
1	University of Dayton ATTN: James M. Whitney 300 College Park Avenue Dayton, OH 45469-0240
1	Purdue University School of Aero and Astro ATTN: C. T. Sun W. Lafayette, IN 47907-1282
1	University of Kentucky ATTN: Lynn Penn 763 Anderson Hall Lexington, KY 40506-0046
3	University of Delaware Center for Composite Materials ATTN: J. Gillespe B. Pipes M. Santare 201 Spencer Laboratory Newark, DE 19716
2	North Carolina State University Civil Engineering Department ATTN: W. Rasdorf L. Spainhour P.O. Box 7908 Raleigh, NC 27696-7908

No. of Copies	Organization
1	University of Utah Department of Mechanical and Industrial Engineering ATTN: S. Swanson Salt Lake City, UT 84112
1	Stanford University Department of Aeronautics and Aeroballistics Durant Building ATTN: S. Tsai Stanford, CA 94305
1	Pennsylvania State University ATTN: Renata S. Engel 245 Hammond Building University Park, PA 16801
1	Pennsylvania State University ATTN: David W. Jensen 223-N Hammond University Park, PA 16802
1	Pennsylvania State University ATTN: Richard McNitt 227 Hammond Bldg. University Park, PA 16802
1	UCLA MANE Dept., Engrg IV ATTN: H. Thomas Hahn Los Angeles, CA 90024-1597
1	University of Illinois at Urbana-Champaign National Center for Composite Materials Research 216 Talbot Laboratory ATTN: J. Economy 104 South Wright Street Urbana, IL 61801
1	Virginia Polytechnic Institute and State University Engineering Science and Mechanics Department ATTN: M. W. Hyer Blacksburg, VA 24061-0219
2	Olin Corporation Flinchbaugh Division ATTN: E. Steiner B. Stewart P.O. Box 127 Red Lion, PA 17356

No. of Copies	Organization
1	Chamberlain Manufacturing Corporation Research and Development Division ATTN: T. Lynch 550 Esther Street P.O. Box 2335 Waterloo, IA 50704
1	Olin Corporation ATTN: L. Whitmore 10101 9th St., North St. Petersburg, FL 33702
3	Alliant Techsystems, Inc. ATTN: C. Candland J. Bode K. Ward 5640 Smetana Drive Minnetonka, MN 55343
1	Alliant Techsystems, Inc. Precision Armaments Systems Group 7225 Northland Drive Brooklyn Park, MN 55428
1	Virginia Polytechnic Institute and State University Engineering Science and Mechanics Department ATTN: M. W. Hyer Blacksburg, VA 24061-0219
1	Custom Analytical Engineering Systems, Inc. ATTN: A. Alexander Star Route, Box 4A Flintstone, MD 21530
2	Institute for Advanced Technology ATTN: T. Kiehne H. Fair 4030-2 W. Braker Lane Austin, TX 78759
2	Kaman Sciences Corporation ATTN: D. Elder J. Betz P.O. Box 7463 Colorado Springs, CO 80933

No. of Copies	Organization
3	LORAL/Vought Systems ATTN: G. Jackson K. Cook L. L. Hadden 1701 West Marshall Drive Grand Prairie, TX 75051
1	Interferometrics, Inc. ATTN: R. Larriva, Vice President 8150 Leesburg Pike Vienna, VA 22100
1	ARMTEC Defense Products ATTN: Steve Dyer 85-901 Avenue 53 P.O. Box 848 Coachella, CA 92236

USER EVALUATION SHEET/CHANGE OF ADDRESS

This Laboratory undertakes a continuing effort to improve the quality of the reports it publishes. Your comments/answers to the items/questions below will aid us in our efforts.

1. ARL Report Number ARL-TR-105 Date of Report May 1993

2. Date Report Received _____

3. Does this report satisfy a need? (Comment on purpose, related project, or other area of interest for which the report will be used.) _____

4. Specifically, how is the report being used? (Information source, design data, procedure, source of ideas, etc.) _____

5. Has the information in this report led to any quantitative savings as far as man-hours or dollars saved, operating costs avoided, or efficiencies achieved, etc? If so, please elaborate. _____

6. General Comments. What do you think should be changed to improve future reports? (Indicate changes to organization, technical content, format, etc.) _____

CURRENT ADDRESS

_____
Organization

_____
Name

_____
Street or P.O. Box No.

_____
City, State, Zip Code

7. If indicating a Change of Address or Address Correction, please provide the Current or Correct address above and the Old or Incorrect address below.

OLD ADDRESS

_____
Organization

_____
Name

_____
Street or P.O. Box No.

_____
City, State, Zip Code

(Remove this sheet, fold as indicated, tape closed, and mail.)
(DO NOT STAPLE)

DEPARTMENT OF THE ARMY

OFFICIAL BUSINESS

BUSINESS REPLY MAIL
FIRST CLASS PERMIT No 0001, APG, MD

Postage will be paid by addressee

Director
U.S. Army Research Laboratory
ATTN: AMSRL-OP-CI-B (Tech Lib)
Aberdeen Proving Ground, MD 21005-5066

NO POSTAGE
NECESSARY
IF MAILED
IN THE
UNITED STATES